water

MDPI

*Article*

# Scour Hole Development in Natural Cohesive Bed Sediment around Cylinder-Shaped Piers Subjected to Varying Sequential Flow Events

**Badal Mahalder [1], John S. Schwartz [2,*], Angelica M. Palomino [2] and Jon Zirkle [3]**

[1] Department of Water Resources Engineering, Faculty of Civil Engineering, Bangladesh University of Engineering and Technology, Dhaka 1000, Bangladesh; bmahalde@vols.utk.edu
[2] Department of Civil and Environmental Engineering, Tickle College of Engineering, The University of Tennessee, Knoxville, TN 37996, USA; apalomin@utk.edu
[3] Tennessee Department of Transportation, 6601 Centennial Blvd, Nashville, TN 37243, USA; Jon.Zirkle@tn.gov
* Correspondence: jschwart@utk.edu; Tel.: +1-865-974-7721

**Abstract:** Scour evolution and propagation around a cylinder in natural cohesive sediment was uniquely investigated under multi-flow event varying sequentially by velocity magnitudes. This flume study differs from others that only used test sediment with commercially available clays for single flow. The objective of this study was to explore the potential differences in scour hole development in natural riverbed sediments subjected to varying flow velocity scenarios, advancing our understanding from existing studies on scour. The study consisted of 18 experimental runs based on: velocity, flow duration, and soil bulk density. Scour hole development progressed initially along the cylinder sides, and maximum depths also occurred at these lateral locations. Scour hole depths were less for higher soil bulk densities ($\geq$1.81 g/cm$^3$) compared with lower densities, and erosion rates were slower. It was observed with all flow sequences that scour depths were similar at the end of each experimental run. However, scour initiation was observed to be time dependent for soils with higher bulk density (1.81–2.04 g/cm$^3$) regardless of flow velocity sequences. The observed time dependency suggests a process feedback with the scour hole development initiated at the cylinder sides, which influence local 3D hydraulics as the scour hole depth progresses.

**Keywords:** cohesive sediments; riverbed scour; cylindrical bridge piers; multiple flow events; equilibrium scour depth



**Citation:** Mahalder, B.; Schwartz, J.S.; Palomino, A.M.; Zirkle, J. Scour Hole Development in Natural Cohesive Bed Sediment around Cylinder-Shaped Piers Subjected to Varying Sequential Flow Events. *Water* **2021**, *13*, 3289. https://doi.org/10.3390/w13223289

Received: 8 October 2021
Accepted: 16 November 2021
Published: 20 November 2021



## 1. Introduction

Improving our understanding of local scour around bridge piers is needed to better manage infrastructure integrity. In the US, during the past 30 years, more than 1000 bridges have failed and about 50–60% of those failures were due to hydraulic forces and bed scour [1–3]. A design manual from the US Federal Highway Administration (FWHA) [4] provides predictive equations for scour at bridge piers and abutments, and generally these equations are well accepted for non-cohesive riverbed sediments. However, this is not the case for cohesive bed sediment and riverbank soils. In addition, few studies have been conducted on cohesive soil scour due to the complex erosion processes of cohesive sediments itself [5–13]. The complexity of these erosion processes is dependent on several factors related to soil physical, geochemical, and biological properties [14]. Particles from cohesive sediment bed begin to mobilize when the magnitude of interparticle bonds is exceeded by the applied stress of moving water. Cohesive soil erosion has several forms: connecting aggregates, flocs, and/or particle by particle [9]. Papanicolaou et al. [15] described incipient soil erosion by fluvial processes as particle removal followed by soil stress–stain relations, and aggregate removal and transport. In general, scour rates in cohesive soils are slow and represent a fatigue failure behavior compared to non-cohesive sediments, where attaining equilibrium scour depth may take several days to years under

multiple flow events [6,16]. Geotechnical properties of the natural soils greatly influence erosion behavior, and the dominant properties vary between physiographic regions [17]. Further research is needed to advance our understanding of the multifaceted interactions between initial scour hole development in cohesive sediments around bridge piers and the hydraulics that promote hole shape and depths over time.

Local scour around bridge piers is dependent on several key factors: stream bed sediment properties, flow conditions, time required for equilibrium scour, and pier characteristics [18–21]. Experimental studies on how these factors influence scour hole development have typically relied on artificial soils and a single flow regime. Studies on artificial test soils have been conducted using mixtures of non-cohesive sediments with commercially available clay at different proportions [6–11]. Critical soil parameters used to predict equilibrium scour depths include clay content (CC) and antecedent moisture content (WC), and these properties differ between artificial and natural soils (in situ conditions) [6,8–11]. Gudavalli [22] conducted an experimental study on commercially available pure clay soils to observe the influence of multiple flow events on scour depth evolution around circular bridge piers and developed a conceptual model for ultimate scour depth predictions using two sets of experiments. Later, the method was modified by Briaud et al. [16]. However, in naturally available cohesive soil, the proportions of sand, silt, and clay content vary based on geological location and origin of a stream. Inherent attractive forces between the clay particles from biological properties occur in natural environments, influencing cohesiveness [14,23]. However, it is nearly impossible to develop the biological parameters in the sediment during the experimental period in a laboratory setting.

The influence of time dependency of scour development in non-cohesive sediment have been considered in numerous studies [24–27]. Several studies have also investigated the influence of flow duration, flow magnitude, and flow frequency on erosion behavior of cohesive soil, including the influence on bank erosion, fluvial erosion (channel incision), and localized scour around structures [28–31]. However, the constant flows used in most cohesive soil scour studies do not represent the flow hydrograph of natural streams/rivers consisting of a rising limb, a peak flow, and a falling limb. Flow duration and peak duration varies based on storm event duration and the characteristics of the watershed. The duration of peak flow may vary and recede afterwards. Therefore, sequences of low-medium-high flows or vice versa is expected in any continuous flow hydrograph over the life span of a bridge, which can produce scour around bridge foundations. Since the scour rate in cohesive soil is relatively slow, it was hypothesized that the influence of stress history from multiple flow events may have significant influence on bed scour depth evolution around cylindrical bridge piers.

The objective of this study was to observe and measure the evolution of scour depths around a cylinder in natural cohesive sediments from multiple flow events where velocities were varied during each experimental run. A review of existing studies and predictive equations are summarized below. Results from the literature indicate the lack of consensus on dominant variables leading to the maximum or equilibrium scour depth. In addition to pier shape, flow velocity and depth as well as cohesive soil properties appear to be important factors. Relevant soil properties include clay content, critical shear stress for incipient erosion, and soil water content [5,6,9–11,16,32,33]. Few studies have focused on the evolution of scour shape and depth near piers as influenced by stress history and a material memory effect. Design equations in the US Federal Highway Administration (FHWA) HEC-18 Manual [34] for bridge piers have been found to produce inconsistent results, as noted in the literature review (Section 2). A critical need exists to improve on the existing predictive equations for scour adjacent bridge piers, particularly with the greater risk imposed from more frequent flooding from climate change.

## 2. Review: Riverbed Scour Depth Equations for Bridge Piers in Cohesive Soils

Equations for prediction of riverbed scour depths in cohesive soil adjacent bridge piers have mostly focused on estimating equilibrium scour depth. Those equations have

been developed with different flow and soil properties using commercially available clay or mixture of clay–sand at different proportions [6,9–11]. From those studies, the relative slowness has been identified in scouring processes compared with non-cohesive soils. Contradictory findings on equilibrium scour depths prediction have also been reported in the literature. For example, similar maximum scour depths for both non-cohesive and cohesive sediments under similar flow conditions have been reported [5,7]. Other studies have reported lower or even higher maximum scour depths for cohesive soils compared to non-cohesive soils [8,9,24–28].

Molinas and Hosny [6] recommended equations for estimating geometric dimensions of scour hole and maximum scour depths based on the observed scour volume using three sets of laboratory flume experiments. They proposed an equation for clay–sand mixture with less than 31% clay–slit proportions:

$$\frac{y_s}{D} = 18.92\left(\frac{F_r^{2.08}}{(1+C)^{1.88}}\right) \tag{1}$$

where $y_s$ is the maximum scour depth, $D$ is the pier diameter, $C$ is the fraction of cohesive soil, and $F_r$ is the Froude number, which should be in the range of 0.18–0.33.

Briaud et al. [5] introduced a new method for scour prediction in cohesive soils by introducing the time-dependent scour depth prediction using a hyperbolic equation. They reported that maximum shear stress at a pier is calculated based on the initial erosion rate obtained from erosion function apparatus (EFA) tests. They proposed a generalized curve was developed based on different soil types to predict the initial erosion rate for different maximum shear stress ($\tau_{max}$) values at a pier. The proposed equation for estimating $\tau_{max}$ value was given as [5]:

$$\tau_{max} = 0.094\rho V^2\left(\frac{1}{\log R_p} - \frac{1}{10}\right) \tag{2}$$

where $\tau_{max}$ is the maximum shear stress at the pier; $\rho$ is the density of water; $V$ is the approach flow velocity; and $R_p$ is the pier Reynolds number. The time dependent scour depth is then calculated using the following formula:

$$y_t = \frac{t}{\frac{1}{z_i} + \frac{t}{y_s}} \tag{3}$$

where $t$ is the time of scour; $z_i$ is the initial erosion rate calculated using the $\tau_{max}$ value; and $y_s$ is the maximum scour depth calculated using the following functional relationship with $Rp$:

$$y_s = 0.018R_p^{0.635} \tag{4}$$

This method is applicable for circular pier with deep water condition and constant flow velocity.

Considering the flow variation in natural streams, this method was further modified based on a series of experiments. Briaud et al. [16,32] modified the equation for incorporating the influence of shallow water effect, attack-angle effect, pier shape effect, and pier spacing effect. The modified equations of maximum shear stress and maximum scour depth with the correction factors are as follows:

$$\tau_{max} = k_w k_{sp} k_{sh} k_a 0.094\rho V^2\left(\frac{1}{\log \frac{Vb}{\nu}} - \frac{1}{10}\right) \tag{5}$$

$$y_s = k_w k_{sp} k_{sh} 0.018R_p^{0.635} \tag{6}$$

where $b$ is the projected pier width perpendicular the flow; $k_w$, $k_{sp}$, and $k_a$ are the correction factor for shallow water, pier spacing, and angle of attack, respectively.

$$k_w = \begin{cases} 0.85\left(\frac{h}{b}\right)^{0.34} & \text{for } \frac{h}{b} < 1.62 \\ 1 & \text{for } \frac{h}{b} > 1.62 \end{cases} \quad (7)$$

Debnath and Chaudhuri [9–11] conducted series of flume experiments on clay–sand mixed sediment at different WC and clay content. Based on the experimental data, Debnath and Chaudhuri [9] proposed regression equations to estimate the dimensionless maximum scour depth at circular pier founded in clay sand mixed bed:

$$\hat{y}_s = 2.05{F_{rp}}^{1.72}C^{-1.29}{\hat{\tau}_s}^{-0.37} \text{ for } WC = 20 - 23.22\% \text{ and } 20\% \le C \le 85\% \quad (8)$$

$$\hat{y}_s = 3.64{F_{rp}}^{0.22}C^{-1.01}{\hat{\tau}_s}^{-0.69} \text{ for } WC = 27.95 - 33.55\% \text{ and } 20\% \le C \le 50\% \quad (9)$$

$$\hat{y}_s = 20.52{F_{rp}}^{1.28}C^{0.19}{\hat{\tau}_s}^{-0.89} \text{ for } WC = 27.95 - 33.55\% \text{ and } 50\% \le C \le 100\% \quad (10)$$

$$\hat{y}_s = 3.32{F_{rp}}^{0.72}C^{-0.62}WC^{0.36}{\hat{\tau}_s}^{-0.29} \text{ for } WC = 33.60 - 45.92\% \text{ and } 20\% \le C \le 70\% \quad (11)$$

$$\hat{y}_s = 8{F_{rp}}^{0.61}C^{058}WC^{1.24}{\hat{\tau}_s}^{-0.19} \text{ for } WC = 33.60 - 45.92\% \text{ and } 70\% \le C \le 100\% \quad (12)$$

where $\hat{y}_s$ is the dimensionless maximum scour depth $\left(\hat{y}_s = \frac{y_s}{D}\right)$; $F_{rp}$ is the pier Froude number; C is the clay content; $\hat{\tau}_s$ is the dimensionless bed shear stress $\hat{\tau}_s = \frac{\tau_s}{\rho V^2}$; and $\tau_s$ is the vane shear strength of the soil.

Briaud et al. [33] further updated the pier scour equation for cohesive material by incorporating the critical velocity for initiation of erosion, which was added to HEC-18 [34] report and expressed as:

$$y_s = 2.2K_1K_2D^{0.65}\left(\frac{2.6V - V_c}{\sqrt{g}}\right) \quad (13)$$

where $y_s$ is the maximum scour depth; $K_1$ and $K_2$ are the correction factor for pier shape and angle of attack, respectively; $D$ is the pier diameter; $V$ is the flow velocity; $V_c$ is the critical flow velocity for scour initiation; and g is the gravitational acceleration. However, Briaud et al. [33] recommend that Equation (3) should be used for calculating time-dependent scour development.

Milonas and Hosny [6] and Debnath and Chaudhuri [9] equations were developed for maximum scour depth prediction only. Briaud et al. [15,33,34] equations considered the time dependent scour development in addition to the maximum scour depth prediction. In the later stage, a generalized curve developed by Briaud et al. [33], which was used for estimating initial erosion rate ($z_i$) based on soil type. However, they recommended applying the EFA for developing erosion rate curve for the test soils. In this study, the observed scour depths from each flow events were compared with the predicted scour depths using the hyperbolic time dependent scour formula developed by Briaud et al. [5]. The FWHA HEC-18 [34] equation, Equation (13), was also used for maximum scour depth prediction with the experimental condition to observe the possible variations among these sets of equations.

## 3. Experimental Set-Up and Procedures

### *3.1. Flume Construction*

For this experimental study, a 12.20 m long, 1.22 m wide, and 0.61 m deep outdoor flume was constructed at the University of Tennessee, Knoxville on the East Tennessee AgResearch and Education Center (ETREC) property (Figure 1). The sides and bottom of this flume were constructed with plywood material and a geo-liner was used as a water

seal. A test section (1.22 m × 1.22 m × 0.3 m) was constructed 8.23 m downstream from the flume entrance (Figure 1). Water was pumped from a nearby slough of the Tennessee River using a 6-inch suction pump (0.13 $m^3/s$ maximum flow capacity (United Rental Inc., Stamford, CT, USA). The desired flow velocity was maintained with the variable control system attached to the pump. The slope of the flume was kept constant at 0.85%.

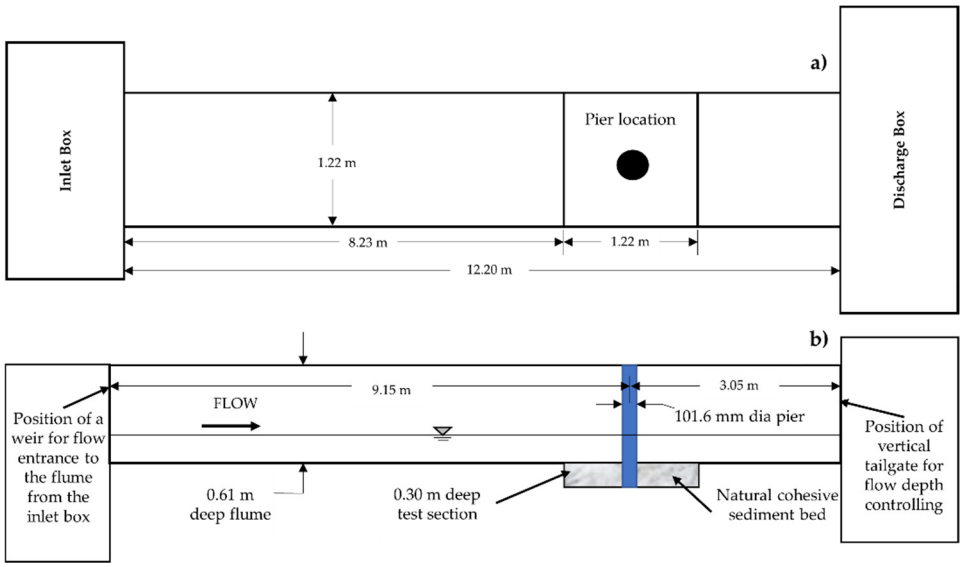


**Figure 1.** Detail of the flume: (**a**) plan view, and (**b**) long section of the flume (not to scale).

### *3.2. Properties of Natural Cohesive Sediment*

In this experimental study, natural cohesive sediments were used for each flow condition. The sediment samples were collected from streambanks of Crooked Creek, Shelby County, Tennessee, USA. The geological properties of this stream site are described in detail in Mahalder et al. [17]. The in-situ WC and bulk density (BD) of the sediment were 23.82% and 2.04 $g/cm^3$, respectively. The details of other sediment properties are reported in Table 1.

**Table 1.** Sediment properties of the natural cohesive soil used in this study.

| Properties | |
|---|---|
| Median grain size (μm) | 12.00 |
| Liquid limit, LL | 29.00 |
| Plastic limit, PL | 18.95 |
| Plasticity index, PI | 10.05 |
| In-situ moisture content (%) | 23.82 |
| In-situ cohesion (kPa) | 67.56 |
| Sand % | 3.00 |
| Silt % | 72.00 |
| Clay % | 25.00 |
| Clay activity | 0.41 |
| Specific surface area ($m^2/g$) | 46.49 |
| Sodium adsorption ration (SAR) | 5.34 |
| Potassium intensity factor (KIF) | 0.07 |
| Field bulk density, BD ($g/cm^3$) | 2.04 |
| Specific gravity | 2.658 |
| Geometric standard deviation ($\sigma_g$) | 9.83 |

The cohesive soil collected for the study had approximately 72% silt and 25% clay. A standard proctor test was conducted on the collected soil after remolding, which showed the maximum density was obtained at a much lower WC than the in-situ WC. Replicating

the exact in-situ soil conditions (e.g., in-situ density at the in-situ WC) is difficult given the variations of physical properties between remolded and in-situ soils. Therefore, the test sediment beds were prepared by targeting desired BD values and measuring the corresponding WC values rather than compacting the soil to the optimum WC.

### *3.3. Sediment Bed Preparation*

Three different compaction efforts were applied to prepare sediment beds for this experimental study. For matching the field BD of the sediment bed, water was spread over the dry soil and covered for 24 h for hydrating the soil uniformly. The moist soil was then placed in the test box and compacted in three approximately equal lifts. Each layer was compacted with a 25.4 cm × 25.4 cm cast iron tamper dropped manually ~30 cm above the lift surface. After compaction, a 16 kg roller was used to smooth out the surface and avoid any possible kneading in the soil for attaining desired BD. Two core samples were collected from each lift for WC and BD measurements using the standard method. A 101.6 mm diameter clear Plexiglass cylinder was inserted in the middle of the test section acting as a circular bridge pier (Figure 2a,b). Figure 2a shows the locations of vertical graduated tape strips glued to the inner surface of the cylinder at different circumference locations (counter-clockwise: 0° (front), 45 °, 90° (right side), 135 °, 180° (back), 270° (left side), 225 °, and 315 °) for periodic scour depth measurements.

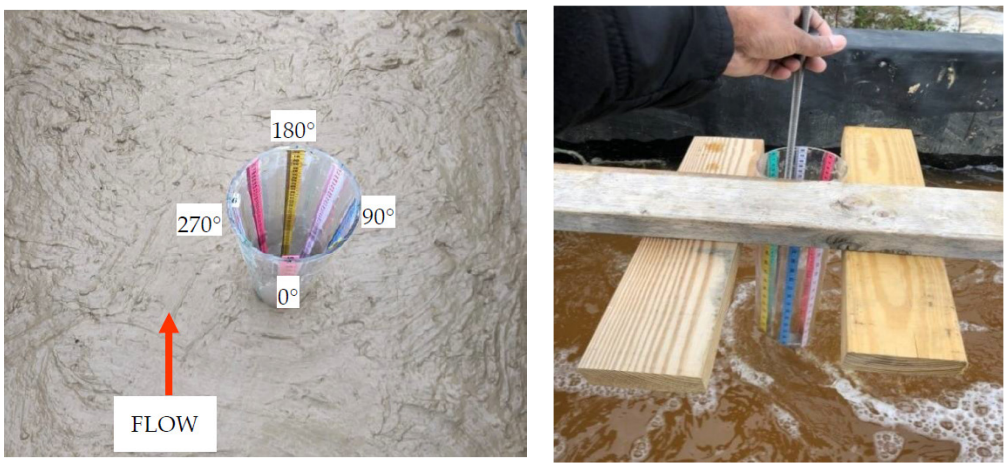


(**a**) (**b**)

**Figure 2.** (**a**) Prepared sediment bed with the Plexiglas circular pier, and (**b**) placement of underwater camera during experiments for periodic scour depth measurement.

Experiments were also conducted on sediment beds with three other BD values: BD = 1.81–1.86 g/cm$^3$ (higher density), BD = 1.69–1.71 g/cm$^3$ (medium density), and BD = 1.52–1.56 g/cm$^3$ (low density). For the first set of targeted BD values, the soil was mixed thoroughly by hand with water then the moistened soil was placed into the test section. The soil was then compacted using the tamper for attaining the desired BD. The low-density sediment bed was prepared by adding more water to the soil and compacting by hand using a wooden board to achieve the target density. The sediment beds were compacted in three layers. After preparing the sediment bed, the critical shear stress ($\tau_c$) was measured at two downstream locations using a mini-jet device following the standard mini-jet operation procedures. Soil shear strength was also measured using a hand-held vane shear instrument (E-286 Inspection Vane, Omnimetrix, Saint-Laurent, QC, Canada) at four to five locations (ASTM D2573, Saint-Laurent, QC, Canada). The top surface of the prepared sediment bed was levelled gently by hand using a trowel. The prepared sediment bed was then kept covered for 16–24 h before conducting an experiment. For each experiment set, a fresh sediment bed was prepared following similar procedures (Table 2).

**Table 2.** Experimental conditions for 18 scenarios based on flow velocity and duration, soil bulk density (BD), and soil water content (WC).

| Experimental Set | Run No | Flow Condition | Flow Velocity (cm/s) | Duration (Hours) | BD (g/cm$^3$) | WC |
|---|---|---|---|---|---|---|
| **1** | 1 | Low | 81.25 | 36 | 2.04 | 25.31 |
| | 2 | High | 102.20 | 36 | 2.03 | 25.31 |
| **2** | 3 | Low | 79.98 | 12 | 1.84 | 30.16 |
| | 4 | Medium | 89.41 | 12 | 1.84 | 30.16 |
| | 5 | High | 100.34 | 12 | 1.84 | 30.16 |
| **3** | 6 | Low | 80.40 | 12 | 1.71 | 37.86 |
| | 7 | Medium | 91.25 | 12 | 1.71 | 37.86 |
| | 8 | High | 100.60 | 12 | 1.71 | 37.86 |
| **4** | 9 | High | 102.40 | 12 | 1.86 | 31.25 |
| | 10 | Medium | 90.26 | 12 | 1.86 | 31.25 |
| | 11 | Low | 80.36 | 12 | 1.86 | 31.25 |
| **5** | 12 | High | 101.40 | 12 | 1.69 | 38.12 |
| | 13 | Medium | 89.52 | 12 | 1.69 | 38.12 |
| | 14 | Low | 80.10 | 12 | 1.69 | 38.12 |
| **6** | 15 | Low | 81.25 | 36 | 1.81 | 31.24 |
| **7** | 16 | Low | 80.68 | 36 | 1.56 | 37.45 |
| **8** | 17 | High | 99.89 | 36 | 1.83 | 30.65 |
| **9** | 18 | High | 100.26 | 36 | 1.52 | 37.90 |

Note: Approach flow depth, h = 15.25 cm and cylinder diameter = 10.16 cm.

### *3.4. Experimental Procedures*

This experimental study was conducted in a shallow water condition ($h/D$ = 1.50) for attaining higher velocities during experiments. During several trial runs, it was determined that at least 70 cm/s depth average velocity was required for observing any scour depths around the cylinder for an experimental run over 12 h. For attaining flow velocities higher than 70 cm/s, a 15.25 cm water depth was maintained throughout these experiments by controlling the tailgate height. In these experiments, flow type was subcritical. Since the flume boundary was smooth, the mean velocity profile was approximated by the log law [35]. A handheld SonTek/YSI ADV (San Diego, CA, USA, Version 2.5) was used for velocity measurements at different points during experimental runs. Depth average mean velocity was approximated by measuring the velocity using the handheld ADV at 0.2 y and 0.8 y depths and averaging the values [7,11]. Depth-wise velocity distributions for three different flow conditions are presented in Figure 3.

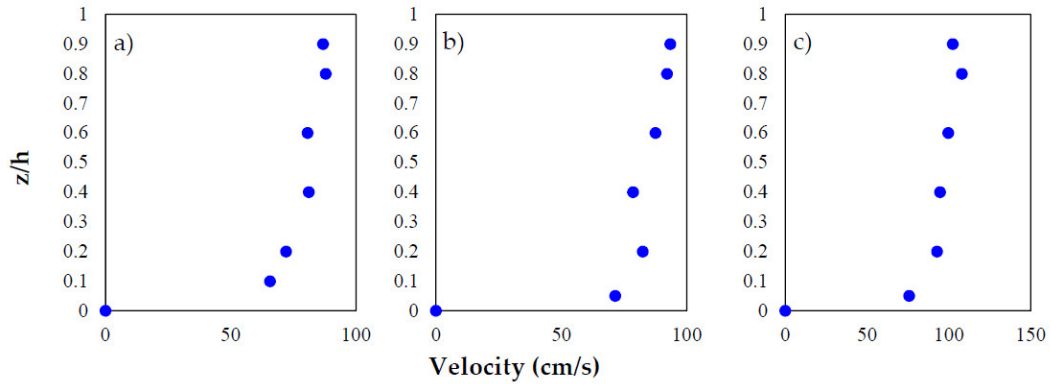


**Figure 3.** Velocity distribution with depth: (**a**) low flow (run no. 3), (**b**) medium flow (run no. 4), and (**c**) high flow (run no. 5).

The objective of this experiment was to observe the scour depth evolution and progress under multiple flow events using different flow sequences. During each experimental

run, flow depth was monitored throughout using graduated tape attached to the sides of the flume at different locations. For the above-mentioned soil conditions, different flow velocity sequences: Low (0.79–0.82 m/s), Medium (0.89–0.92 m/s), and High (>0.99 m/s) were used in this experimental study as presented in Table 2. A total of 18 experimental runs were conducted comprising nine different scenarios using natural cohesive sediment. During each experimental run, an underwater camera was used for capturing periodic pictures and videos of the scour depths as developed on the graduated tapes attached inside the cylinder. After finishing each experimental run, the water was drained out from the scour hole and detailed measurements were conducted using a point gage mounted on the top of the flume.

## 4. Results and Discussion

### *4.1. Evolution of Scour Depth around Cylinder*

The development of large secondary flow and skewed velocity distributions around pier create downward negative pressure gradient normal to the flow direction, which separates the flow at the pier and forms the horseshoe vortex. Horseshoe vortex propagates in the downstream direction (~2 to 3 times of pier diameter), past the sides of the pier, and becomes part of the turbulence, which initiates the scour development [36–38]. In this study, scour depth measurements around the cylinder showed that for a given experimental run, scour initiated at the left or right sides (either 90° or 270° with flow direction) of the cylinder. The maximum scour developed at the left or right side of the cylinder except for one scenario (experimental run #4), where maximum scour depth was between 45° and 90° of the cylinder (Table 3). Similar findings have been reported in other studies [7,9–11,13,39].

**Table 3.** Scour depth development around circular pier for different flow velocities and soil properties.

| Run No | Location of Max Scour Depth | | Observed Scour Depth around the Sides of Pier (cm) | | | | | | | | Lateral Extent of Scour Hole around the Pier, $X_L$ (cm) | | | | | | | |
|---|---|---|---|---|---|---|---|---|---|---|---|---|---|---|---|---|---|---|
| | After Each Flow | End of Test | 0° | 45° | 90° | 135° | 180° | 225° | 270° | 315° | 0° | 45° | 90° | 135° | 180° | 225° | 270° | 315° |
| **1** | 90° | 90° | 0.50 | 1.40 | 2.20 | 2.00 | 1.20 | 0.60 | 0.60 | 0.30 | 4.57 | 7.62 | 11.43 | 5.08 | 10.16 | 3.81 | 4.10 | 4.57 |
| **2** | 90° | 270° | 0.50 | 2.90 | 3.10 | 3.00 | 1.10 | 1.50 | 1.00 | 1.60 | 3.60 | 7.25 | 9.80 | 10.26 | 17.00 | 12.25 | 5.60 | 6.25 |
| **3** | 90° | | 0.20 | 0.60 | 0.70 | 0.40 | 0.40 | 0.60 | 0.60 | 0.40 | 2.60 | 2.51 | 2.60 | 3.50 | 6.60 | 3.60 | 2.40 | 3.20 |
| **4** | 270° | 90° | 1.00 | 1.30 | 0.90 | 1.10 | 0.30 | 0.80 | 1.40 | 1.00 | 2.70 | 3.20 | 3.00 | 3.50 | 7.12 | 4.00 | 3.60 | 3.50 |
| **5** | 90° | | 0.50 | 1.50 | 2.50 | 1.30 | 0.80 | 0.80 | 2.20 | 1.40 | 3.50 | 5.00 | 4.00 | 4.00 | 8.15 | 7.25 | 4.20 | 4.00 |
| **6** | 45° | | 1.70 | 3.10 | 1.90 | 0.20 | 0.50 | 0.50 | 1.70 | 1.20 | 3.00 | 4.50 | 3.00 | 4.50 | 4.00 | 8.00 | 6.00 | 3.00 |
| **7** | 270° | 45° | 0.40 | 0.70 | 0.90 | 1.30 | 0.50 | 1.00 | 1.50 | 0.90 | 3.00 | 4.50 | 6.00 | 8.00 | 14.00 | 9.00 | 7.00 | 5.50 |
| **8** | 45° | | 0.70 | 2.90 | 1.50 | 1.20 | 0.30 | 1.50 | 1.00 | 1.00 | 4.50 | 5.00 | 6.50 | 11.00 | 17.00 | 13.00 | 8.00 | 8.00 |
| **9** | 270° | | 1.30 | 1.50 | 2.00 | 1.80 | 1.50 | 1.50 | 3.00 | 2.00 | 1.50 | 2.00 | 3.00 | 9.00 | 12.00 | 4.00 | 3.00 | 2.00 |
| **10** | 90° | 270° | 0.20 | 1.00 | 1.00 | 1.10 | 0.90 | 1.60 | 0.60 | 1.00 | 4.00 | 2.50 | 5.00 | 14.00 | 23.00 | 8.00 | 6.00 | 4.00 |
| **11** | 270° | | 0.30 | 1.20 | 0.80 | 0.80 | 1.00 | 1.40 | 1.50 | 0.90 | 4.50 | 4.60 | 6.50 | 14.00 | 23.00 | 8.50 | 6.50 | 4.60 |
| **12** | 270° | | 2.10 | 3.50 | 4.00 | 0.70 | 1.20 | 2.00 | 4.30 | 4.20 | 4.00 | 2.00 | 2.60 | 6.00 | 9.00 | 8.00 | 6.00 | 5.00 |
| **13** | 90° | 90° | 0.20 | 0.70 | 1.10 | 1.00 | 0.30 | 1.00 | 1.00 | 1.00 | 5.00 | 2.00 | 3.50 | 11.00 | 11.00 | 9.00 | 7.00 | 6.00 |
| **14** | 90° | | 1.00 | 0.50 | 2.20 | 1.50 | 0.70 | 1.00 | 0.70 | 0.50 | 5.00 | 3.00 | 6.00 | 12.00 | 12.00 | 12.00 | 8.00 | 6.00 |
| **15** | 90° and 270° | | 1.10 | 2.10 | 3.20 | 1.20 | 1.50 | 2.10 | 3.20 | 2.20 | 3.50 | 6.20 | 8.00 | 10.80 | 11.30 | 8.60 | 6.20 | 5.00 |
| **16** | 90° | | 2.60 | 5.80 | 6.40 | 3.90 | 2.70 | 5.30 | 4.80 | 4.80 | 6.00 | 10.00 | 8.50 | 14.00 | 9.00 | 4.50 | 5.00 | 4.00 |
| **17** | 90° and 270° | | 2.00 | 3.70 | 5.30 | 4.10 | 2.60 | 3.00 | 5.30 | 3.40 | 6.00 | 5.50 | 11.50 | 18.50 | 13.00 | 12.00 | 8.00 | 5.00 |
| **18** | 90° | | 4.50 | 6.80 | 9.00 | 8.00 | 1.40 | 5.20 | 6.60 | 4.80 | 6.50 | 9.00 | 14.00 | 11.00 | 7.00 | 5.00 | 5.50 | 5.00 |

Note: Approach flow depth, h = 15.25 cm and cylinder diameter, D = 10.16 cm.

Experimental results from this study demonstrated that the progression of scour depths was also dependent on the BD values. In the wake zone (downstream side of the cylinder), the lateral and transverse extent of the scour hole was larger compared with other sides of the cylinder (Figure 4). In further analyzing of the scouring processes around the cylinder, scouring initiated at the sides (90° and 270° with the flow) and gradually propagated either in the upstream or downstream directions for all cases. Overall, scour depths at the nose of the pier (0°) were greater compared with the scour depths at the wake zone (180°) for all 18 experimental runs.

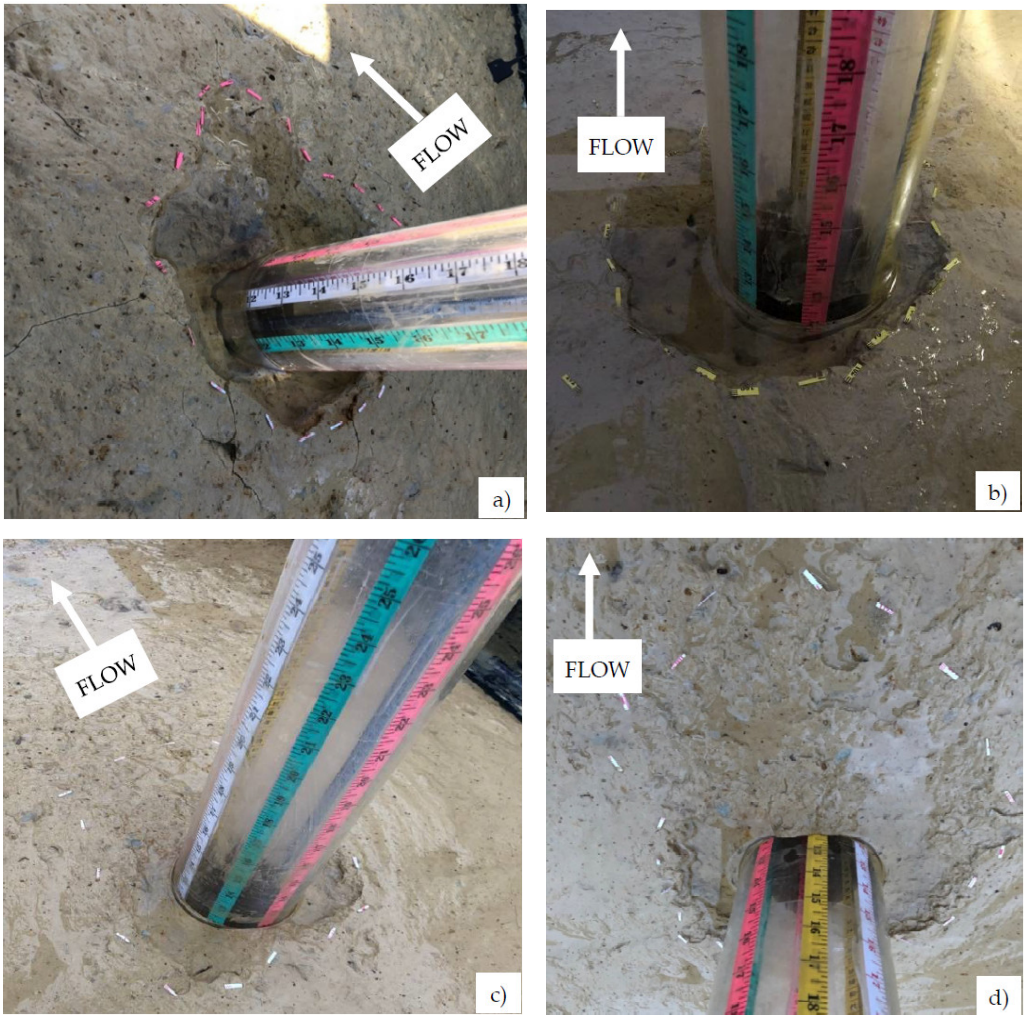


**Figure 4.** Scour hole development for (**a**) run 16, V = 80.68 cm/s, WC = 37.45%, (**b**) run 14, V = 80.10 cm/s, WC = 38.12%, (**c**) run 10, V = 90.26 cm/s, WC = 31.25%, and (**d**) run 9, V = 102.40 cm/s, WC = 31.25%.

Ting et al. [7] reported that at lower $R_p$ values, the formation of scour depths on the downstream side and upstream side of pier were similar; however, at higher $R_p$ values, the downstream side (wake region) scour depth was more, compared with the upstream side (nose of the pier) scour depth. However, Debnath and Chaudhuri [9] argued that the Ting et al. [7] observations may not always be valid during the scour depth propagation. They reported that the insufficient bed shear stress development during experimental run could also produce different scour depths at the upstream and downstream side of a pier. Therefore, they identified that in addition to the $R_p$ values, $\tau_{max}$ (calculated using Equation (5)) has strong influence on the scour depth propagation towards either the downstream or the upstream side of cylinder. In this study, the calculated $\tau_{max}$ values were significantly greater (6.38–9.76 N/m$^2$) compared to those in the Ting et al. [7] study (2.26–4.83 N/m$^2$), and $R_p$ values ranged between $6.6 \times 10^4$ and $9.8 \times 10^4$. However, in this study, the scour depths were found to propagate predominantly towards the downstream side of the cylinder compared with upstream side for all flow and BD conditions.

Observations from this study deviated from the results reported by Debnath and Chaudhuri [9]. Rather, the results from this study are more consistent with those of Ting et al.'s [7] observations of scour propagation in cohesive sediments. However, greater scour depths were observed at the nose of the cylinder (0°) compared with back side (180°) of the cylinder. It was assumed that the upstream turbulent flow was forcing the horseshoe vortex to move around the downstream side of the pier; consequently, soil layer

was removed from the downstream area compared with other locations (Figure 5). In addition, due to the shallow water condition, as the depth of the scour hole increases the water loses its eroding energy faster [32,39,40]. Consequently, the sidewise propagation of the scour hole was prominent at the downstream side. The cohesive strength of soil likely also influenced scour propagation. Since a natural cohesive sediment was used in this study, the cohesion developed quicker in the soil compared with the commercially available completely remolded clay soils.


**Figure 5.** Scour hole development and the soil removal erosion pattern at the wake zone of the pier: run 14, V = 80.10 cm/s, WC = 38.12%.

Scour depths did not propagate at the same rate for the entire experiment duration according to the scour depth data around the cylinder (Table 3). Both down-cutting and widening in scour holes were observed with time rather than deepening at the same location. The pressure gradient as developed in the scour holes and the uneven shear stress distribution in the scour hole due to shallow depth condition appear to have influenced the growth of scour holes. The maximum scour hole developed at the sides (90° or 270° with the flow) of the cylinder after the initial flow period, which also influenced the scour propagations on the other sides of the cylinder during the Medium flow condition. Resulting greater scour depth readings were recorded at the other attached graduated tapes rather than formation of deep scour hole in same position. This process continued for the next applied flow events (though at a slower rate), and higher scour depths were then recorded at those locations. However, due to limitations of the pump capacity, another set of flow sequence runs was not tested, suggesting a need for future research for further insight into scour behavior in cohesive sediments.

### *4.2. Influence of Multi-Flow on Scour Propagation*

Most previous studies on bridge scour in cohesive sediments focused on single flow events without considering the influence of flow sequence. In reality, multiple flow events above flow thresholds for scour with different magnitudes, frequency, and duration are expected to occur during the design life of a bridge. Briaud et al. [16] studied and reported the significance of multi-flow events based on two laboratory experiments in commercially-available clay material. They proposed a hyperbolic equation for predicting the time dependent scour depth for different flow events, as discussed in the previous section. Scour depth development and propagation could be affected by the sequence of different flow events. Therefore, in this study, two flow sequences were used: (i) High−Medium−Low (H−M−L), and (ii) Low−Medium−High (L−M−H) on different soil BD conditions for understating cohesive sediment scour (Table 2). Results from this experimental study showed that flow sequence had notable influence on scour depth evolution for different soil BD conditions (Figure 6).

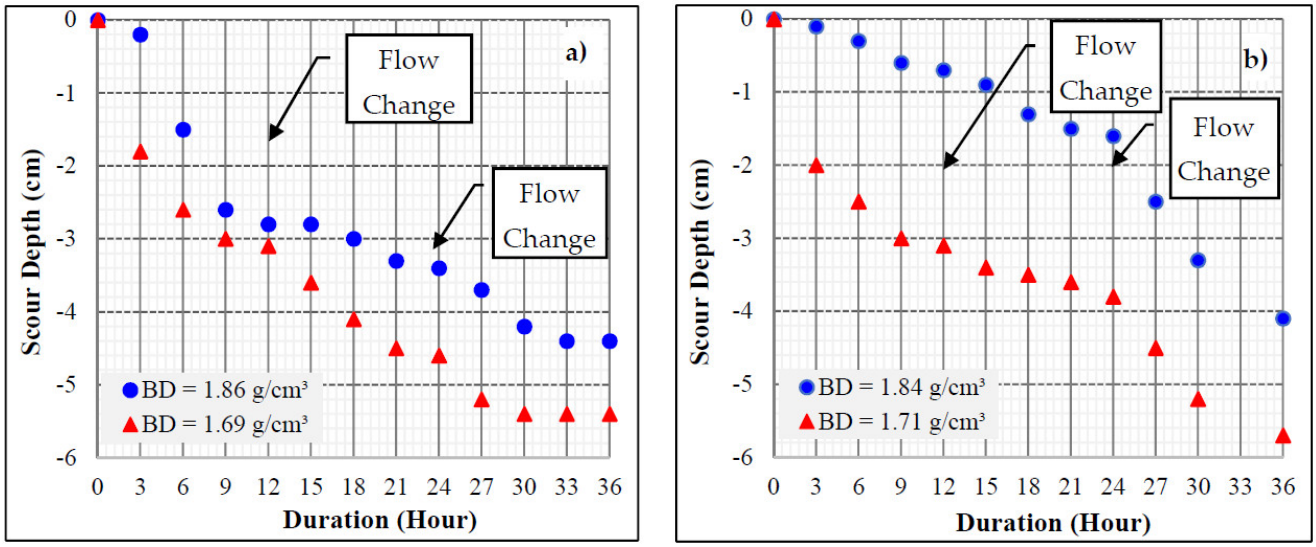


**Figure 6.** The evolution of maximum scour depth: (**a**) for High−Medium−Low (H−M−L) flow sequence at 270° and 90° locations of the pier, (**b**) for Low−Medium−High (L−M−H) flow sequence at 90° and 45° locations of the pier. BD = bulk density of the soil.

Regardless of the flow sequence, similar maximum scour depths were observed for the natural cohesive sediment with BD between 1.69–1.86 g/cm$^3$ at the end of experimental run. For H-M-L flow sequence (Figure 6a), the high flow rate resulted in the highest scour rate, followed by decreased depth change during medium flow, and finally an even lower change in depth for low flow. The scour rate at higher BD (1.86 g/cm$^3$) reduced substantially at the end of high-flow events. For lower BD soil (1.69 g/cm$^3$), higher scour rate was observed at high flow, which reduced significantly during medium flow and increased again at lower flow events. For the L−M−H flow sequence (Figure 6b), the rate of scour depths development was higher during the high flow condition. Development of scour evolution was also studied for high density (BD = 2.03–2.04 g/cm$^3$), medium density (BD = 1.81–1.83 g/cm$^3$) and low density (BD = 1.52–1.56 g/cm$^3$) natural sediments using High−High−High (H−H−H) and Low−Low−Low (L−L−L) flow events (Figure 7). In these experimental runs, the experiment was stopped after 12 h to measure the scour hole depth without disturbing the soil surface, after which the experimental run was restarted. Temporal scour depth measurements showed that for each type of soil, scour rates were reduced after 24 h, except for low density soils at high flows (Figure 7a).

For the case of low density soils (1.51–1.71 g/cm$^3$), scour initiated during the early stage of each experimental run at each flow condition (Figure 7). Examining the recorded pictures and videos during the experimental runs qualitatively, it was observed that for the soft sediment bed, the erosion mechanism was sediment removal particle by particle and removal of individual flocs. As the experimental run time progressed and the scour holes deepened, the soil saturation level played an influential role in removing soil aggregates from scour holes during higher flow conditions. At lower flow velocities, it was assumed that the erosive capacity of the flowing water in the deeper scour hole was not high as very few aggregates were removed. The reduction of effective shear stress in the scour hole could have also influenced the slower scour rate propagation at low flow velocities. It was also assumed that during lower shear stress the erosion pattern was dominated by particle-by-particle removal based on the observation of a smoother scour hole. At high flow velocities, the surface of scour hole was rough suggesting more aggregate mobilization and fluvial transport. Due to the limited pump capacity, flow sequences (L−M−H and H−M−L) were not tested for the dense soil cases since, at low flow, no scour was observed after 12 h of flow (Figure 7b).

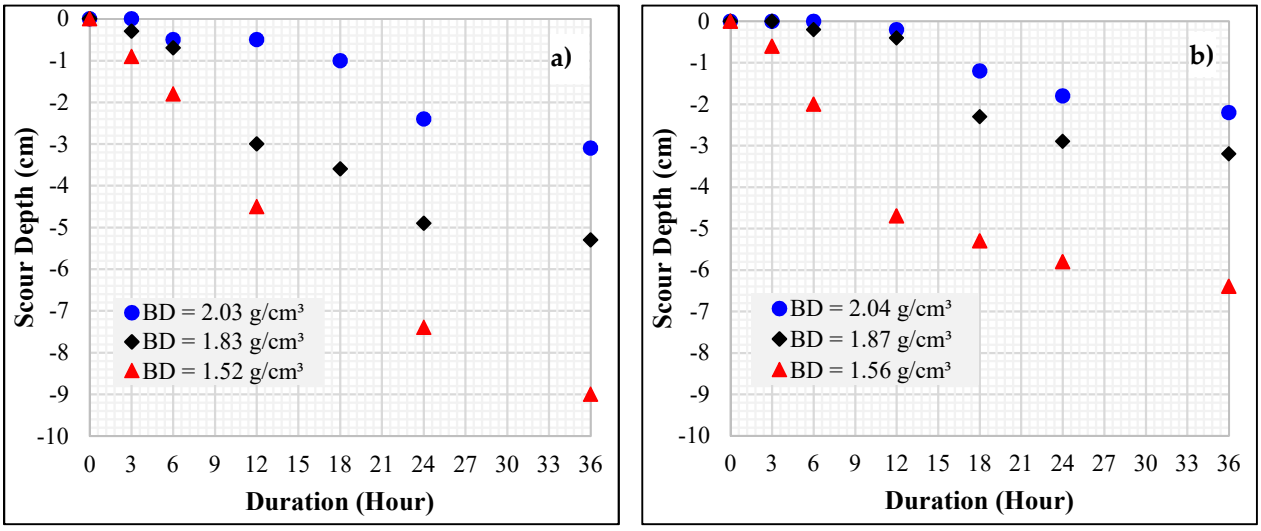


**Figure 7.** The evolution of maximum scour depth: (**a**) for High−High−High (H−H−H) flow sequence at 270° and 90° of the pier, (**b**) for Low−Low−Low (L−L−L) flow sequence at 90° and 270° of the pier.

### *4.3. Influence of Stress History on Scour Propagation*

It has been reported that erosion behavior of soil with high silt–clay content consistent with cohesive sediments is dominated by subaerial processes followed by excess shear stresses resulting in entrainment during a stormflow hydrograph [29,30]. Though the sediment detachment and movement around bridge piers and abutments are fundamentally different from fluvial erosion on streambanks, it was expected that the stress history and associated erosion processes function similarly as the scour propagation around bridge piers. In general, the effect of stress history on scour development was observed from these experimental results since scour depths were not visible immediately after starting experimental runs for the denser soils. Results from this study show that for low density soils, scour initiated immediately after starting an experimental run as reported in the previous section. For soils with higher BDs (1.81–2.04 g/cm$^3$), the time to scour depth initiation depended on flow velocity. At lower flow velocities, scour depths were mostly observed after 12 h, whereas at high flow velocities scour depths initiated 3–6 h after the start of an experimental run.

After the initial period of an experimental run, the rate of scour depth development decreased for both the H−M−L and L−M−H flow sequences at each BD condition (time = 12 to 24 h in Figure 6a,b). The scour rate increased significantly after 24 h (time = 24 to 36 h) regardless of the flow condition, though at higher flow velocities larger scour depths were observed. It was observed that at the end of initial flow, an intermediate equilibrium state was attained. During Medium flow, the scour hole developed from the previous flow event was exposed to either higher or lower shear stresses. These observations also justify the influence of previous stress history on the scour rate propagation during intermediate flow, though relatively lower scour rates were observed for any BD conditions.

In the H−M−L flow sequence, since the previous stress history was higher, a lower scour rate was observed compared with the L−M−H flow sequence. At the end of Medium flow, the scour rate increased regardless of flow sequence used for the last stage of each experiment. Since the scour hole was exposed to a certain shear stress history for a longer period of time, it is likely that the introduction of higher flow events could have influenced the subsequent higher scour rate. In each case, both the shear duration and soil saturation during the experimental period could have influenced the scouring processes. The sour rate was not linear at any stage of the flow sequence.

The influence of repetitive shear forces on the soil surface during both low and high flow conditions was studied at a representative field BD condition (2.03–2.04 g/cm$^3$). At higher flow velocity (>0.99 m/s), less time was required for aggregate removal around

the cylinder compared with low flow velocity (0.79–0.82 m/s), where greater time was required (Figure 7). This observation indicates that a greater exposure time is required for breaking the inter-particle attractive forces between cohesive sediment particles at lower flow velocity. For a higher flow velocity, the required exposure time is smaller for breaking the inter-particle attractive forces. However, soil with lower BDs may behave like non-cohesive sediments as the observed scour progression revealed that scour initiated from the start of the experimental run. Working with completely remolded sediment could have also influenced the scour behavior at lower BD, since the higher WC played a role in sediment dislodgement as the shear strength of soil reduced significantly. This observation suggests that scour rate in remolded cohesive sediment could be significantly different from the in-situ undisturbed consolidated cohesive sediment.

### *4.4. Comparison between Different Scour Depth Equations*

Considering the hydraulics due to flow around the cylinder and the soil properties, maximum scour depths were computed using different scour prediction equations and compared with the observed value from this study. These equations, developed for cohesive sediment scour depth prediction, estimated similar maximum scour depths as the HEC-18 equation, except for the Molinas and Hosny [6] equation (Table 4). Of note, the Debnath and Chaudhuri [9] equation estimated smaller equilibrium scour depths when the soil shear strength was higher compared with other methods. In those methods, soil properties were not considered in the scour depth equation, except Briaud et al.'s [33] equation. Briaud et al. [16,33] also considered the time dependency and multi-flow condition for scour depth predictive equations. In this study, the time dependency and multi-flow sequence on scour development was studied; therefore, results from this study were compared with the Briaud et al. [16,33] predicted scour depths given the flow conditions as discussed before. Results from this study show that Briaud et al. [16,33] methods predicted higher scour depths after each flow condition compared with results as observed from these experimental runs (Figure 8).

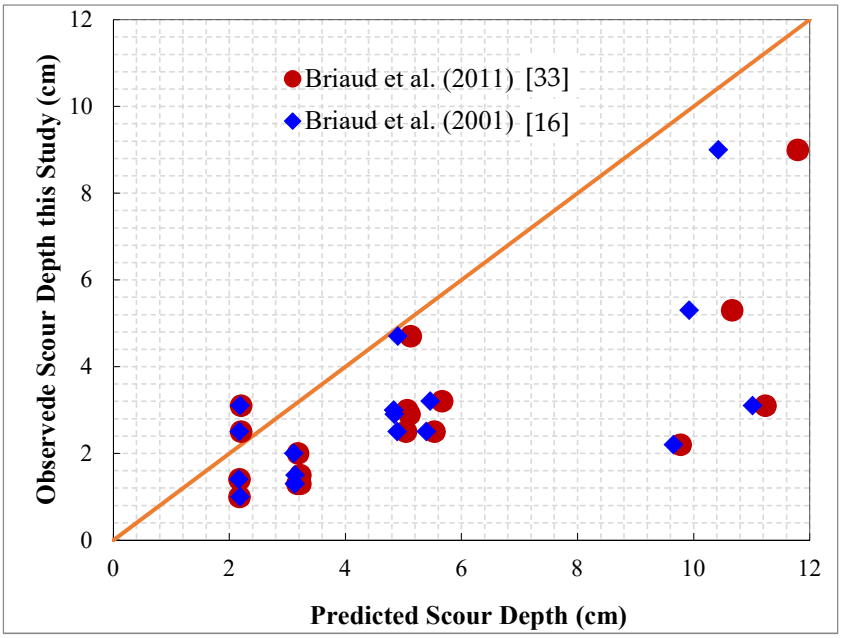


**Figure 8.** Observed and predicted scour depths after each experimental run.

**Table 4.** Comparison of observed scour depths from this study and predicted depths from previous study equations.

| Run No | $\tau_c$ (Pa) | $\tau_s$ (kPa) | Water Temp (°C) | Pier Reynolds No. ($R_p$) | Froude No. ($Fr$) | Observed Max Scour from This Experiment after Each Flow (cm) | Total Maximum Scour after Each Experiment Set (cm) | Estimated Scour Depth (cm) | | | | | | |
|---|---|---|---|---|---|---|---|---|---|---|---|---|---|---|
| | | | | | | | | Molinas and Hosny [6] | Briaud et al. [16] | | Briaud et al. [33] | | Debnath and Chaudhuri, [9] | HEC-18 [34] |
| | | | | | | | | | After Each Flow | Max Scour | After Each Flow | Max Scour | | |
| **1** | 6.65 | 1.36 | 16.50 | 75429 | 0.743 | 2.20 | 2.20 | 64.16 | 9.65 | 23.97 | 9.77 | 21.19 | 13.08 | 20.61 |
| **2** | 6.52 | 1.40 | 17.80 | 98087 | 0.934 | 3.10 | 3.10 | 103.38 | 11.01 | 28.32 | 11.23 | 29.85 | 9.82 | 22.75 |
| **3** | 3.85 | 0.93 | 15.60 | 72521 | 0.731 | 1.00 | | 62.09 | 2.15 | 23.38 | 2.17 | 22.93 | 17.31 | 20.47 |
| **4** | 3.85 | 0.93 | 12.60 | 74759 | 0.817 | 1.30 | 4.10 | 78.28 | 3.13 | 23.84 | 3.17 | 26.82 | 15.21 | 21.48 |
| **5** | 3.85 | 0.93 | 14.40 | 88127 | 0.917 | 2.50 | | 99.51 | 4.89 | 26.46 | 5.04 | 31.34 | 13.31 | 22.57 |
| **6** | 2.35 | 0.62 | 16.50 | 74640 | 0.735 | 3.10 | | 62.76 | 2.18 | 23.81 | 2.20 | 25.81 | 29.51 | 20.52 |
| **7** | 2.35 | 0.62 | 12.10 | 75245 | 0.834 | 1.50 | 6.70 | 81.67 | 3.13 | 23.93 | 3.22 | 30.29 | 30.04 | 21.67 |
| **8** | 2.35 | 0.62 | 10.90 | 80183 | 0.920 | 2.90 | | 100.05 | 4.84 | 24.92 | 5.10 | 34.15 | 30.45 | 22.59 |
| **9** | 3.86 | 0.96 | 9.60 | 78614 | 0.936 | 3.00 | | 103.81 | 4.83 | 24.61 | 5.06 | 32.17 | 12.72 | 22.77 |
| **10** | 3.86 | 0.96 | 10.20 | 70509 | 0.825 | 2.00 | 4.40 | 79.84 | 3.11 | 22.97 | 3.18 | 27.16 | 14.73 | 21.57 |
| **11** | 3.86 | 0.96 | 12.10 | 66265 | 0.735 | 1.40 | | 62.70 | 2.16 | 22.08 | 2.17 | 23.07 | 16.85 | 20.51 |
| **12** | 2.10 | 0.65 | 14.40 | 89058 | 0.927 | 4.70 | | 101.71 | 4.90 | 26.64 | 5.12 | 34.99 | 29.58 | 22.67 |
| **13** | 2.10 | 0.65 | 11.60 | 72785 | 0.818 | 1.30 | 7.30 | 78.48 | 3.12 | 23.43 | 3.22 | 30.09 | 30.11 | 21.49 |
| **14** | 2.10 | 0.65 | 13.40 | 68468 | 0.732 | 2.50 | | 62.28 | 2.17 | 22.54 | 2.20 | 26.20 | 30.53 | 20.49 |
| **15** | 3.67 | 0.96 | 10.20 | 63470 | 0.743 | 2.50 | 2.50 | 64.15 | 5.39 | 21.48 | 5.53 | 23.75 | 16.63 | 20.61 |
| **16** | 2.05 | 0.48 | 13.40 | 68964 | 0.738 | 3.20 | 3.20 | 63.22 | 5.46 | 22.65 | 5.66 | 26.54 | 30.33 | 20.55 |
| **17** | 3.83 | 1.10 | 12.60 | 83522 | 0.913 | 5.30 | 5.30 | 98.58 | 9.92 | 25.58 | 10.66 | 31.19 | 11.91 | 22.53 |
| **18** | 2.28 | 0.48 | 10.60 | 79228 | 0.917 | 9.00 | 9.00 | 99.34 | 10.42 | 24.73 | 11.79 | 34.15 | 30.46 | 22.56 |

Note: Approach flow depth, h = 15.25 cm and cylinder diameter, D = 10.16 cm.

Furthermore, at lower BD (1.51–1.86 g/cm$^3$), the low flow sequence closely predicted the time dependent scour depths in both L−M−H and L−L−L flow sequences. Predicted scour depths (using time-dependent formula) deviated mostly for the intermediate flow condition at higher soil BD. The deviation was also observed for the H−M−L flow sequence, though in this flow sequence, during low flow the predicted scour depths were similar to the observed values from this study. The differences in erosion rates as estimated from the generalized curve by Briaud et al. [33] may have influenced the scour depths estimation Equation (3) for higher flow (Table 4).

Mini-jet tests were conducted in-situ prior to soil sample collection to estimate the average critical shear stress. The in-situ critical shear stress for the soils used in this study ranged between 8.68 to 10.76 Pa. These measurements followed field and analytical analysis described in Mahalder et al. [41]. The critical shear stress of the sediment bed prepared in the laboratory at the field BD condition was 6.52 to 6.65 Pa, which was comparable to the field condition. This result also revealed the influence of soil physical properties on scour development. Briaud et al. [5,16,33] and Ting et al. [7] also identified the influence of soil field conditions on scour development. They suggested that soil field conditions should not be overlooked, therefore, they recommended that soil should be tested in EFA for erosion rate measurement. However, in those studies, ultimate scour depth prediction equations were developed based on commercially available clay soil, which was completely remolded. Properties of field soil samples are likely significantly different from commercially available clay soils. Consequently, the erosion behavior could be different. Debnath and Chaudhuri [9] used field soil samples in their study, which were completely remolded and mixed with sand at different proportions and different WC conditions. However, they did not report any specific scour pattern. Rather, they reported higher shear strength for the field sample.

## 5. Conclusions

This study reports new data on scour around a vertically-positioned cylinder replicating a bridge pier in natural cohesive sediments under multi-flow conditions. The natural cohesive sediment, as used in this study, consists of 3% sand, 72% silt, and 25% clay. The influence of multi-flow events on scour evolution, the influence of previous stress history, and the time-dependent scour development were investigated. Inconsistent findings have been reported by other laboratory flume experiments [5,7–9] on local scour around cylinders in cohesive sediment beds, where either pure clay or mixtures of clay–sand–gravel were used. As observed in this study, scour hole development commenced at the sides of the cylinder and maximum scour depth occurred on the sides of the cylinder (90° or 270°) irrespective of flow velocity and soil BD. For each flow and BD conditions, both the $\tau_{max}$ and $R_p$ values were higher, and larger downstream direction scour propagations were observed. Shallow water conditions (since $h/D < 2.0$) influenced the lateral and transverse scour hole formation at the downstream side of the cylinder compared with two sides and upstream of the cylinder.

Scour propagation under multi-flow conditions showed that, depending on the soil BD, similar maximum scour depths were observed for both the L−M−H and H−M−L flow sequences. Scour rates were found dependent on initial flow velocity and BD, whereas regardless of flow sequence, scour rates were always relatively slow at medium flow velocities. It was also observed that for high soil BD (1.81–2.04 g/cm$^3$), scour depths initiated after 3–12 h of the experimental run. Based on the time-dependent scour development, the available scour prediction equations over-estimated the equilibrium depths. For field soil BD, those equations were estimating substantially higher scour depths, compared with observed scour depths from this study. This finding illustrates that the predicted equilibrium depth for natural cohesive sediment is not similar to non-cohesive sediments, as reported in the literature. Further research through a similar study design specifically targeting more flow events are necessary to better understand the scour development in natural cohesive sediments and development of the equilibrium scour depth equation.

Overall, a better understanding of the scour process around bridge piers is becoming more critical due to increased flooding associated with climate change and the need to protect civil infrastructure.

**Author Contributions:** B.M., the senior author generated the manuscript as part of his PhD dissertation, and co-authors J.S.S., A.M.P. and J.Z. supervised his research, in addition to written text contributions to his study's manuscript. All authors have read and agreed to the published version of the manuscript.

**Funding:** This work was funded by Grant No. RES # 2013-36 from the Tennessee Department of Transportation (TDOT).

**Data Availability Statement:** In this study, all the data have been used are reported in Tables and Figures, as presented in this manuscript.

**Acknowledgments:** The authors would like to thank the reviewers for their comments for improving the manuscript. The authors would also like to thank Andy Baker and Larry Roberts for helping to build the outdoor flume. The authors also appreciate the help from Bobby Simpson, Director, and staff personnel from the ETREC Plant Science Unit of the University of Tennessee, Knoxville for logistics to build the flume and help during experiment run. Student field assistance was provided by Max Carter and Mollika Roy.

**Conflicts of Interest:** The authors declare no conflict of interest.

## References

1. Shirole, A.; Holt, R. Planning for a comprehensive bridge safety assurance program. *Transp. Res. Rec.* **1991**, *1290*, 39–50.
2. Wardhana, K.; Hadipriono, F.C. Analysis of recent bridge failures in the United States. *J. Perform. Constr. Facil.* **2003**, *17*, 144–150. [CrossRef]
3. Cook, W.; Barr, P.J.; Halling, M.W. Bridge failure rate. *J. Perform. Constr. Facil.* **2015**, *29*, 04014080. [CrossRef]
4. FHWA (Federal Highway Administration). National Bridge Inventory. 2012. Available online: https://www.fhwa.dot.gov/bridge/nbi.cfm (accessed on 6 June 2021).
5. Briaud, J.L.; Ting, F.C.K.; Chen, H.C.; Gudavalli, R.; Perugu, S.; Wei, G. SRICOS: Prediction of scour rate in cohesive soils at bridge piers. *J. Geotech. Geoenviron. Eng.* **1999**, *125*, 237–246. [CrossRef]
6. Molinas, A.; Hosny, M.M. Experimental study on scour around circular piers in cohesive soil. In *Publication No. FHWA-RD-99-186, Federal Highway Administration*; U.S. Department of Transportation: McLean, VA, USA, 1999.
7. Ting, F.C.K.; Briaud, J.L.; Chen, H.C.; Gudavalli, R.; Perugu, S.; Wei, G. Flume tests for scour in clay at circular piers. *J. Hydraul. Eng.* **2001**, *127*, 969–978. [CrossRef]
8. Ansari, S.A.; Kothyari, U.C.; Ranga Raju, K.G. Influence of cohesion on scour around bridge piers. *J. Hydraul. Res.* **2002**, *40*, 717–729. [CrossRef]
9. Debnath, K.; Chaudhuri, S. Laboratory experiments on local scour around cylinder for clay and clay–sand mixed bed. *Eng. Geol.* **2010**, *111*, 51–61. [CrossRef]
10. Debnath, K.; Chaudhuri, S. Bridge pier scour in clay–sand mixed sediments at near-threshold velocity for sand. *J. Hydraul. Eng.* **2010**, *136*, 597–609. [CrossRef]
11. Debnath, K.; Chaudhuri, S. Local scour around noncircular piers in clay-sand cohesive sediment beds. *Eng. Geol.* **2012**, *151*, 1–14. [CrossRef]
12. Kothyari, U.C.; Kumar, A.; Jain, R.K. Influence of cohesion on river bed scour in wake region of piers. *J. Hydraul. Eng.* **2014**, *14*, 1–13. [CrossRef]
13. Hamidifar, H.; Omid, M.H. Local scour of cohesive beds downstream of a rigid apron. *Can. J. Civ. Eng.* **2017**, *44*, 935–944. [CrossRef]
14. Grabowski, R.C.; Droppo, I.G.; Wharton, G. Erodibility of cohesive sediment: The importance of sediment properties. *Earth Sci. Rev.* **2011**, *105*, 101–120. [CrossRef]
15. Papanicolaou, A.N.; Wilson, C.G.; Tsakiris, A.G.; Sutarto, T.E.; Bertrand, F.; Rinaldi, M.; Dey, S.; Langendoen, E. Understanding mass fluvial erosion along a bank profile: Using PEEP technology for Quantifying Retreat Lengths and Identifying Event Timing. *Earth Surf. Process Landf.* **2017**, *42*, 1717–1732. [CrossRef]
16. Briaud, J.L.; Chen, H.C.; Kwak, K.W.; Han, S.W.; Ting, F.C.K. Multiflood and multilayer method for scour rate prediction at bridge piers. *J. Geotech. Geoenviron. Eng.* **2001**, *127*, 114–125. [CrossRef]
17. Mahalder, B.; Schwartz, J.S.; Palomino, A.M.; Zirkle, J. Relationships between physical-geochemical soil properties and erodibility of streambanks among different physiographic provinces of Tennessee, USA. *Earth Surf. Process Landf.* **2018**, *43*, 401–416. [CrossRef]
18. Hosny, M.M. Experimental Study of Local Scour around Circular Bridge Piers in Cohesive Soils. Ph.D. Dissertation, Civil Engineering Department, Colorado State University, Fort Collins, CO, USA, 1995.

19. Melville, B.M.; Cheiw, Y.M. Time scale for local scour at bridge piers. *J. Hydraul. Eng.* **1999**, *125*, 59. [CrossRef]
20. Kwak, K. Prediction of Scour Depth Versus Time for Bridge Piers in Cohesive Soils in the Case of Multi-Flood and Layered Soil Systems. Ph.D. Dissertation, Department of Civil Engineering, Texas A&M University, College Station, TX, USA, 2000.
21. Devi, Y.S.; Barbhuiya, A.K. Bridge pier scour in cohesive soil: A review. *Sadhana* **2017**, *42*, 1803–1819. [CrossRef]
22. Gudavalli, R.S. Prediction Model for Scour Rate around Bridge Piers in Cohesive Soil on the Basis of Flume Tests. Ph.D. Dissertation, Civil Engineering Department, Texas A&M University, College Station, TX, USA, 1997.
23. Black, K.S.; Tolhurst, T.J.; Paterson, D.M.; Hagerthey, S.E. Working with natural cohesive sediments. *J. Hydraul. Eng. ASCE* **2002**, *128*, 2–8. [CrossRef]
24. Chang, W.Y.; Lai, J.S.; Yen, C.L. Evolution of Scour Depth at Circular Bridge Piers. *J. Hydraul. Eng.* **2004**, *130*, 905–913. [CrossRef]
25. Pizarro, A.; Tubaldi, E. Quantification of Modelling Uncertainties in Bridge Scour Risk Assessment under Multiple Flood Events. *Geosciences* **2019**, *9*, 445. [CrossRef]
26. Simarro, G.; Fael, C.M.S.; Cardoso, A.H. Estimating Equilibrium Scour Depth at Cylindrical Piers in Experimental Studies. *J. Hydraul. Eng.* **2011**, *137*, 1089–1093. [CrossRef]
27. Liang, B.; Du, S.; Pan, X.; Zhang, L. Local scour for vertical piles in steady currents: Review of mechanisms, influencing factors and empirical equations. *J. Mar. Sci. Eng.* **2020**, *8*, 4. [CrossRef]
28. Wolman, M.G. Factors influencing erosion of a cohesive river bank. *Am. J. Sci.* **1959**, *257*, 204–216. [CrossRef]
29. Costa, J.E.; O'Connor, J.E. Geomorphically effective floods. In *Natural and Anthropogenic Influences in Fluvial Geomorphology*; Geophysical Mono-graph 89: The Wolman Volume; Costa, J.E., Miller, A.J., Potter, K.W., Wilcock, P.R., Eds.; American Geophysical Union: Washington, DC, USA, 1995; pp. 45–56.
30. Julian, J.P.; Torres, R. Hydraulic erosion of cohesive riverbanks. *Geomorphology* **2006**, *76*, 193–206. [CrossRef]
31. Keaton, J.R.; Mishra, S.K.; Clopper, P.E. Scour at bridge foundations on rock. In *National Cooperative Highway Research Program (NCHRP)*; Report 717; Transportation Research Board of National Academics: Washington, DC, USA, 2012.
32. Briaud, J.L.; Chen, H.C.; Nurtjahyo, P. SRICOS-EFA method for complex piers in fine-grained soils. *J. Geotech. Geoenvir. Eng.* **2004**, *130*, 1180–1191. [CrossRef]
33. Briaud, J.L.; Chen, H.C.; Chang, K.A.; Oh, S.J.; Chen, S.; Wang, J.; Li, Y.; Kwak, K.; Nartjaho, P.; Gudaralli, R.; et al. *The SRICOS-EFA Method. Summary Report*; Texas A&M University: College Station, TX, USA, 2011.
34. US DOT FHWA. *Evaluating Scour at Bridges*, 5th, ed.; Hydraulic Engineering Circular No. 18, Publication No. FHWA-HIF-12-003; National Highway Institute: Arlington, VA, USA, 2012.
35. Nezu, I.; Nakagawa, H. *Turbulence in Open-Channel Flows*; Balkema: Rotterdam, The Netherlands, 1993.
36. Melville, B.W.; Raudkivi, A.J. Flow Characteristics in Local Scour at Bridge Piers. *J. Hydraul. Res.* **1977**, *15*, 373–380. [CrossRef]
37. Ballio, F.; Bettoni, C.; Franzetti, S. A survey of time-averaged characteristics of laminar and turbulent horseshoe vortices. *J. Fluid Eng.* **1998**, *120*, 233–242. [CrossRef]
38. Chaudhuri, S.; Debnath, K. Observations on initiation of pier scour and equilibrium scour hole in cohesive sediments. *J. Hydraul. Eng.* **2013**, *19*, 27–37. [CrossRef]
39. Li, J.; Qi, M.; Fuhrman, D.R.; Chen, Q. Influence of turbulent horseshoe vortex and associated bed shear stress on sediment transport in front of a cylinder. *Exp. Therm. Fluid Sci.* **2018**, *97*, 444–457. [CrossRef]
40. Schlömer, O.; Herget, J.; Euler, T. Boundary condition control of fluvial obstacle mark formation—framework from a geoscientific perspective. *Earth Surf. Process. Landf.* **2020**, *45*, 189–206. [CrossRef]
41. Mahalder, B.; Schwartz, J.S.; Palomino, A.M.; Zirkle, J. Estimating erodibility parameters for streambanks with cohesive soils using the mini jet test device: A comparison of field and computational methods. *Water* **2018**, *10*, 304. [CrossRef]